Top Catal (2008) 47:148–154
DOI 10.1007/s11244-007-9026-3

ORIGINAL PAPER

Electrochemically Assisted Photocatalysis of Hybrid WO_3/TiO_2 Films: Effect of the WO_3 Structures on Charge Separation Behavior

Shinya Higashimoto · Yoshiaki Ushiroda · Masashi Azuma

Published online: 14 February 2008
© Springer Science+Business Media, LLC 2008

Abstract In this study, the photocatalysis of hybrid WO_3/TiO_2 films with different loadings of WO_3 were investigated with and without potential bias. It was clearly indicated that hybrid WO_3/TiO_2 films show less photoreactivity under only UV-irradiation, while more effective photocatalysis under potential bias than either TiO_2 or WO_3 by themselves, their photocatalytic performance depending on the loadings of WO_3. In particular, a hybrid WO_3/TiO_2 film involving an amorphous-like WO_3 phase plays a significant role in an enhancement of the electrochemically assisted photocatalysis.

Keywords WO_3/TiO_2 · Electrochemically assisted photocatalysis · Band structure

1 Introduction

Since the effect of Honda–Fujishima on the photocatalysis of TiO_2 was discovered [1], different kind of semiconductor photocatalysts have been extensively studied by many researchers [2–7]. In particular, TiO_2 is interesting as photocatalyst, photoinduced super-hydrophilic materials, while tungsten trioxide (WO_3) as photo-anode, electro- or photochromic materials and photocatalyst [8–14]. In recent years, a considerable attention has been paid to photo-electrochemical properties of the WO_3/TiO_2 double layers, such as photocatalysis, photochromism, and photo-rechargeable battery [15–20]. Under the band gap excitation of WO_3 and/or TiO_2 layers by themselves, photoinduced electrons transfer to the conduction band of WO_3 layers, while holes transfer to the valence band of TiO_2 layers. So that, they play a significant role in maximizing the photocurrent generation efficiency to promote charge separation by accumulating electrons and holes in two different semiconductor layers with suppression of charge recombination.

Our present study deals with electrochemically assisted photocatalysis of hybrid WO_3/TiO_2 film electrodes with different loadings of WO_3. Special attention has been focused on effect of the band structures of an amorphous-like WO_3 or a polycrystalline WO_3 coupled with TiO_2, on the charge separation behavior under UV-irradiation.

S. Higashimoto (✉) · Y. Ushiroda · M. Azuma
Department of Applied Chemistry, College of Engineering, Osaka Institute of Technology, 5-16-1 Omiya, Asahi-ku, Osaka 535-8585, Japan
e-mail: higashimoto@chem.oit.ac.jp

2 Experimental Details

2.1 Film Preparation

TiO_2 (anatase structure) and tungstic acid (H_2WO_4) were purchased from Kanto Chemicals, and ammonium tungstate, $(NH_4)_{10}W_{12}O_{41}\cdot 5H_2O$ was purchased from Kishida Chemicals. Four different types of WO_3-based solid films were prepared by the following procedures: (1) WO_3/TiO_2 samples with different WO_3 loadings were prepared by an impregnation of an aqueous solution of ammonium tungstate into TiO_2. The obtained powder was mixed with triethyleneglycol to form slurry, and it was spread on a conductive indium tin oxide glass (ITO, 10 Ω/square) by squidgie method, followed by thermal treatment at 773 K for 15 min in air, and labeled as x-WO_3/TiO_2 (x represents weight percent of WO_3); (2) A polycrystalline WO_3 material was prepared by thermal decomposition of ammonium tungstate at 873 K for 6 h in air. The polycrystalline WO_3 powder was treated in the same manner on an ITO glass, followed by thermal treatment in air at 773 K

for 15 min, and labeled as c-WO_3; 3) A physically mixed powder (40 wt.% as WO_3) containing both 0.6 g of TiO_2 and 0.4 g of c-WO_3 was treated in the same manner on an ITO glass, followed by thermal treatment in air at 773 K for 15 min, and labeled as 40c-WO_3/TiO_2; 4) The tungstic acid was also treated in the same manner on an ITO glass, followed by thermal treatment at 573 K for 15 min in air, and labeled as a-WO_3. The mass of each film was adjusted to be about 1.5 mg cm^{-2} on an ITO glass unless the mass of film was especially mentioned.

2.2 Film Characterization

Scanning Electron Microscopy (SEM) images were taken at 20 kV accelerating voltage in a JEOL JSM-840A. Atomic Force Microscopy (AFM) images were obtained in a Shimadzu SPM-9500J by tapping mode using an etched silicon tip. The X-ray diffraction (XRD) patterns were obtained with a RIGAKU RINT2000 using Cu K_α radiation ($\lambda = 1.5417$ Å) in a scan range of 20–40° and a scan speed of 2° min^{-1}. The UV–Vis spectroscopic measurements in diffuse reflectance mode were carried out using a Shimadzu UV–Vis recording spectrophotometer, UV-2200A. The collected data were transformed using the Kubelka–Munk function.

2.3 Photoelectrochemical Measurements

Photoelectrochemical measurements were carried out by a Potentiostat/Galvanostat (HABF 5001, HOKUTO DENKO) in a standard two-compartment cell in which three electrodes were connected by the bridge as shown in Fig. 1. The $I-V$ characteristics of film electrodes were obtained at the potential sweep rate of 10 mV s^{-1}. Black light of the fluorescent lamp (0.53 mW·cm^{-2} at 365 nm) was used for photoirradiation of the films. The electrolyte solution was used for 0.5 M Na_2SO_4 aqueous solution involving 0.5 M HCOOH. Also, the pH of aqueous solutions was adjusted by aqueous solutions of H_2SO_4 or NaOH. They were bubbled with N_2 gas for 30 min under vigorous stirring before use. The products after photoreaction were analyzed by gas chromatography equipped with a thermal conductivity detector (TCD) for the analysis of CO_2.

3 Results and Discussion

SEM and AFM images from top views of a 40-WO_3/TiO_2 film was observed as shown in Fig. 2. The film was seen to form the secondary particle having porous surface by an aggregation of the primary particles from the SEM image. Electrolyte solutions involving formic acid can be easily penetrated into the porous film, which is expected to exhibit high photocatalytic activity. The AFM image of 40-WO_3/TiO_2 shows that this film consists of secondary particles (about 300–1,000 nm in diameter) that are in contact with each other.

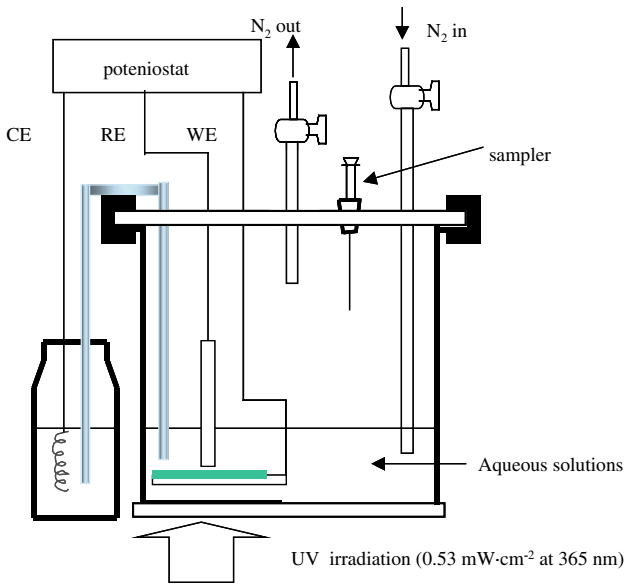

Fig. 1 Schematic diagram of two-compartment cell employed in electrochemically assisted photocatalysis. (CE: Pt wire, RE: Ag/AgCl electrode, WE: film electrode)

Figure 3 shows X-ray diffraction patterns of WO_3/TiO_2 films with different loadings of WO_3. Structural change of WO_3 was observed to transform from an amorphous-like structure to a polycrystalline structure as an increase of WO_3 on TiO_2, that is, 20- and 40-WO_3/TiO_2 involve an amorphous-like WO_3 phase, whose diffraction pattern is similar with that of a-WO_3, while 60-WO_3/TiO_2 and 40c-WO_3/TiO_2 involve a polycrystalline WO_3 as a major phase [20]. Here, an amorphous-like WO_3 structure can be defined to be as the intermediate between an amorphous WO_3 and a polycrystalline WO_3.

The photocurrent responses as a function of applied potentials ($I-V$ characteristics) for film electrodes under photoirradiation and in dark are shown in Fig. 4. Firstly, the saturated photocurrent was obtained at +1.0 V vs. Ag/AgCl. Secondly, a flatband potential of the film was defined to be as a zero photocurrent potential, i.e., the photocurrent can be seen at more anodic potential, while no more effect of electrochemical intercalations of protons are observed at more cathodic than the flatband potential.

Influence of film thickness on the saturated photocurrent at +1.0 V versus Ag/AgCl is shown in Fig. 5. The photocurrent for each film electrodes was saturated at more than 1.5 mg cm^{-2} of film mass. Given the condition of the

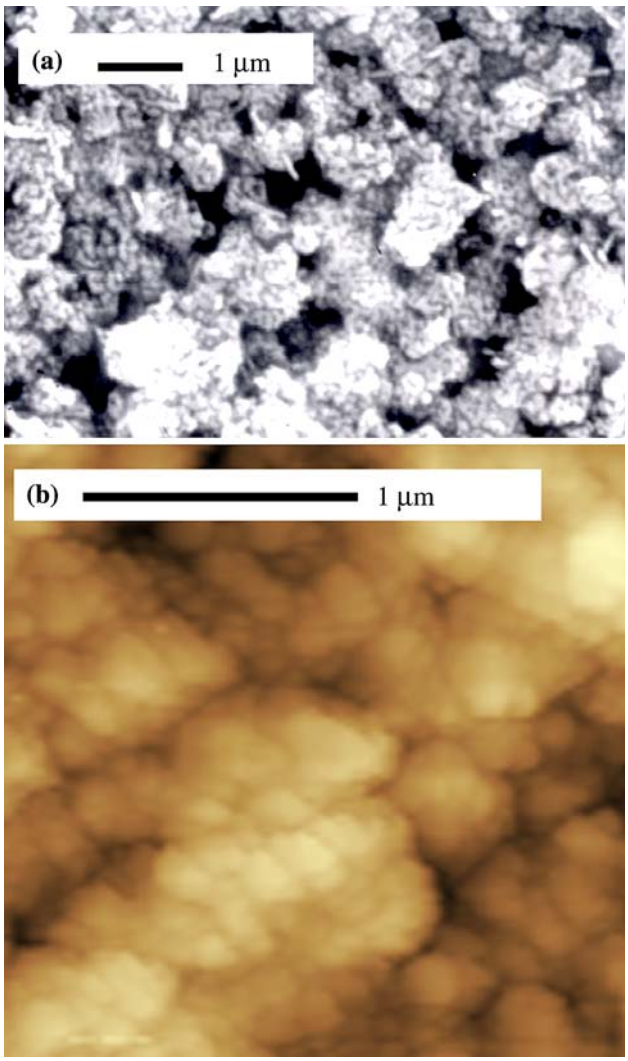

Fig. 2 SEM and AFM micrographs from top views of 40-WO_3/TiO_2 (**a** and **b**)

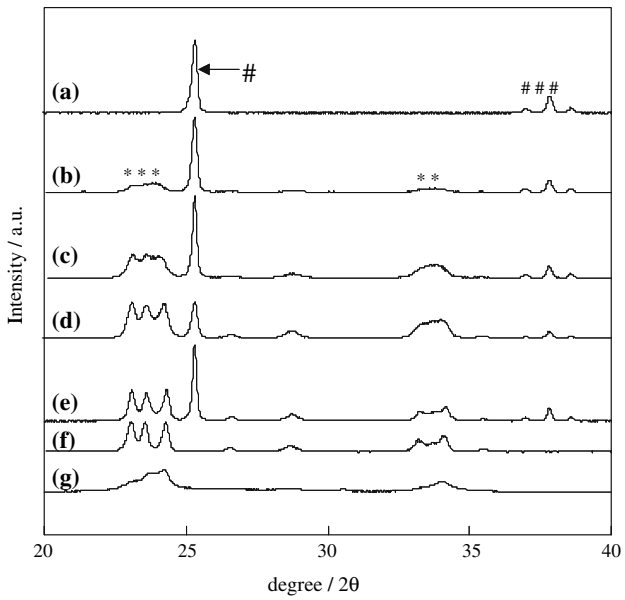

Fig. 3 XRD patterns of TiO_2 (**a**), 20-, 40-, 60-WO_3/TiO_2 (**b–d**), 40c-WO_3/TiO_2 (**e**), c-WO_3 (**f**) and a-WO_3 (**g**) (*: WO_3; #: anatase TiO_2)

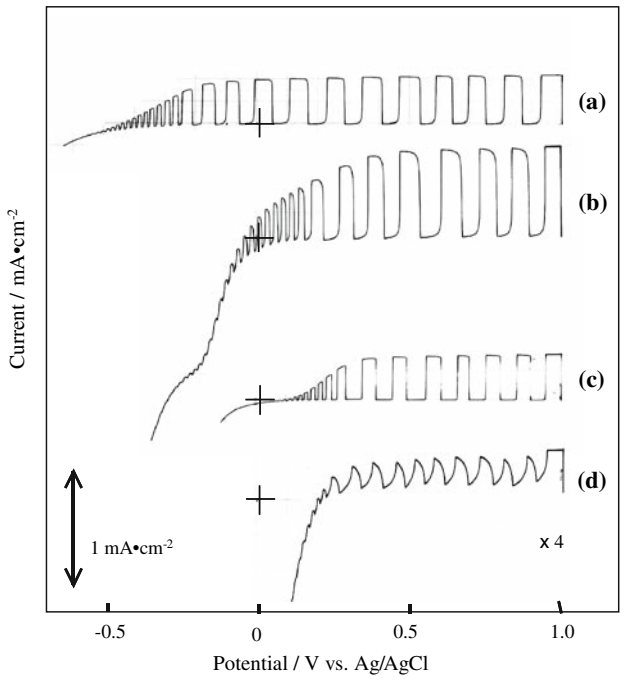

Fig. 4 Dependence of the photocurrent as a function of applied voltage ($I-V$ characteristics) under UV-irradiation (up) and in dark (down): TiO_2 (**a**), 40-WO_3/TiO_2 (**b**), c-WO_3 (**c**) and a-WO_3 (**d**). The pH of an aqueous solution was adjusted at 2.1

saturated photocurrent of the film electrodes, it was found that (1) the photocurrent efficiency depend on loadings of WO_3 on TiO_2, and was maximized at 40 wt.% WO_3 and then decreased at loadings higher than 60 wt.%; (2) 40c-WO_3/TiO_2 exhibits lower photocurrent efficiency than either WO_3 or TiO_2 by themselves as shown in Fig. 6.

Figure 6 also shows the yields of CO_2 for the photocatalytic decomposition of formic acid under UV-irradiation with or without potential bias at +1.0 V versus Ag/AgCl. With no bias, all of the hybrid WO_3/TiO_2 film electrodes exhibit lower photocatalytic activity than either TiO_2 or WO_3 by themselves. On the other hand, under potential at +1.0 V versus Ag/AgCl, UV-irradiation of hybrid WO_3/TiO_2 film electrodes show higher photocatalytic activity than either TiO_2 or WO_3 by themselves, while it was found to be maximized at 60 wt.% WO_3 and then decreased at loadings higher than 40 wt.%, which corresponds with the efficiency of the saturated photocurrent. In fact, this profile can be explained by the transformation from an amorphous-like WO_3 (at ~40 wt.%) to a polycrystalline WO_3 structure (60~ wt.%) as evidenced by the XRD data as shown in Fig. 3. Furthermore, 40c-WO_3/TiO_2 was seen to exhibit lower efficiency for the electrochemically assisted

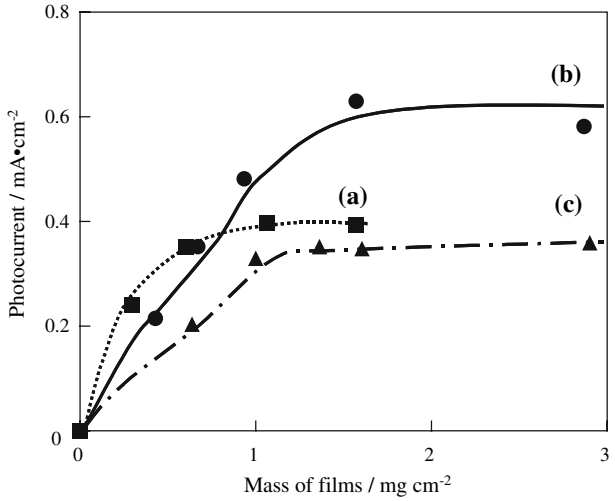

Fig. 5 Dependence of the saturated photocurrent density as a function of mass of films for TiO_2 (**a**), 40-WO_3/TiO_2 (**b**), and c-WO_3 (**c**). The pH of an aqueous solution was adjusted at 2.1

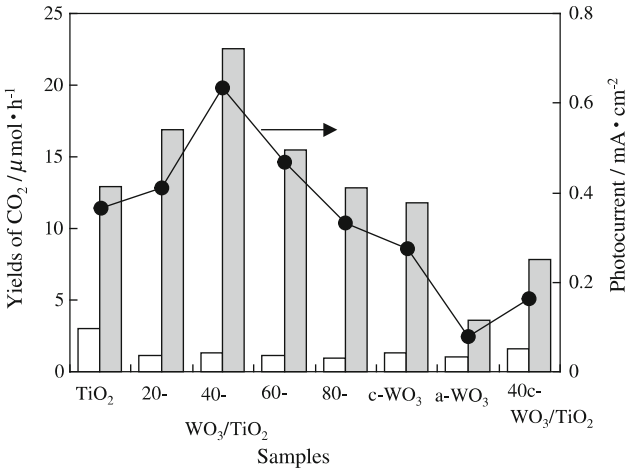

Fig. 6 Yields of CO_2 photo-formed with (gray bar) and without (white bar) potential bias at +1.0 V versus Ag/AgCl, and saturated photocurrent density (black circle). The pH of an aqueous solution was adjusted at 2.1

photocatalysis than 40-WO_3/TiO_2. These results indicate that the hybrid WO_3/TiO_2 film having an amorphous-like WO_3 can play an important role in more effective charge separation than the film having a polycrystalline WO_3 on photo-electrochemical cells.

Figure 7 shows the potential shifts of photocharge under UV-irradiation, and discharge under dark condition. Photocharged potentials were saturated at around −0.49 V for TiO_2, −0.29 V for 40-WO_3/TiO_2, +0.03 V for a-WO_3 and +0.03 V for c-WO_3 versus Ag/AgCl, respectively, under UV-irradiation for 60 min, while 40-WO_3/TiO_2 and a-WO_3 exhibit blue coloration. When light is turned off, both of TiO_2 and c-WO_3 exhibit rapid self-discharge and/or discharge, while photocharged 40-WO_3/TiO_2 and a-WO_3 exhibit a typical Faradic discharge behavior (bleaching color) by galvanostatic discharge at the rate of 10 μA cm^{-2}.

Photocharge and discharge processes are associated with intercalation of protons into WO_3 to form tungsten bronze (H_xWO_3) and deintercalation of protons, respectively, accordingly to the following process of (1) [17, 19, 21].

$$WO_3 + xe^- + xH^+ \underset{\text{discharge}}{\overset{\text{photocharge}}{\rightleftarrows}} H_xWO_3 \quad (1)$$

Moreover, XRD data clearly indicate that tungsten bronze (H_xWO_3) (x: 0.23 or 0.33) is formed through the intercalation of protons depending on the photocharged potentials. The reason for the suppression of the photoreactivity of the hybrid WO_3/TiO_2 films under no bias can be explained by the formation of tungsten bronze.

Figure 8 shows the linear correlation between the pH of aqueous solutions and the flatband potentials (U_{fb}) on TiO_2, 40-WO_3/TiO_2 and WO_3 film electrodes. The flatband potentials of TiO_2 and WO_3 film electrodes follow the theoretical equation of (2) through (de)protonation on the surface. The E^0 and pH in the equation of (2) represent the flatband potential at pH = 0 and the pH of aqueous solutions, respectively. Such phenomena were also observed in a hybrid WO_3/TiO_2 film electrode, suggesting that it also gives a property of metal-oxide semiconductor such as WO_3 and TiO_2.

$$U_{fb} = E^0 - 0.059\ \text{pH} \quad (2)$$

The flatband potentials of WO_3 coupled with TiO_2 depend on the loadings of WO_3 on TiO_2, and they shift

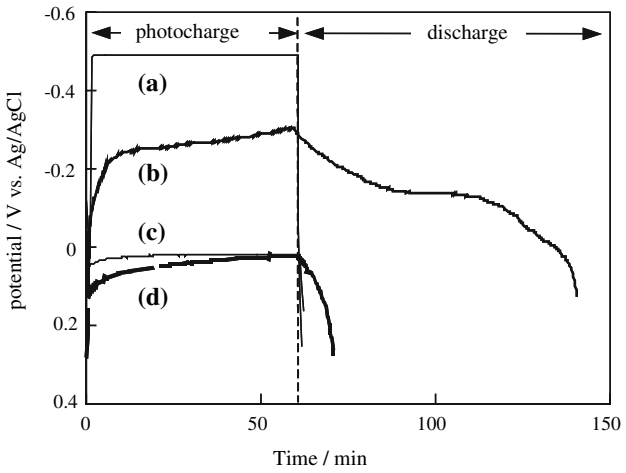

Fig. 7 Changes in potential by photocharge for 60 min, and subsequently galvanostatic discharge at 10 μA·cm^{-2} on TiO_2 (**a**), 40-WO_3/TiO_2 (**b**), c-WO_3 (**c**) and a-WO_3 (**d**). The pH of an aqueous solution was adjusted at 2.1

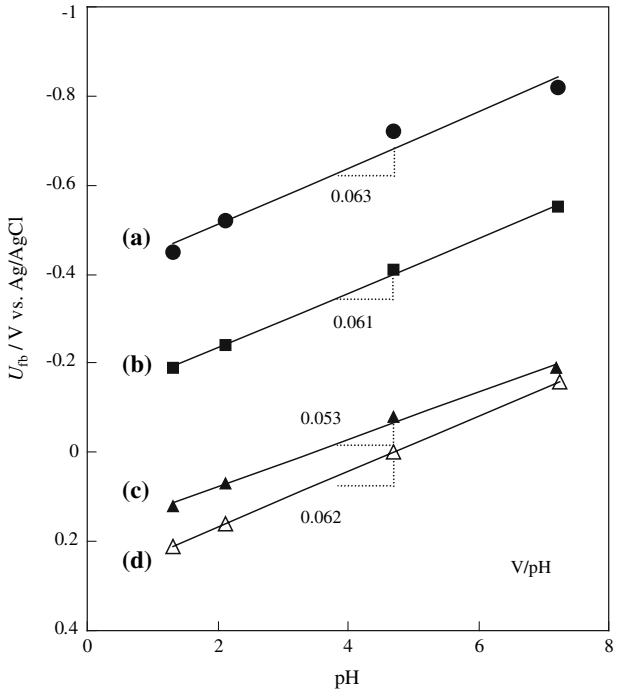

Fig. 8 Dependence of the pH of aqueous solutions on the flatband potentials for TiO_2 (**a**), 40-WO_3/TiO_2 (**b**), c-WO_3 (**c**) and a-WO_3 (**d**)

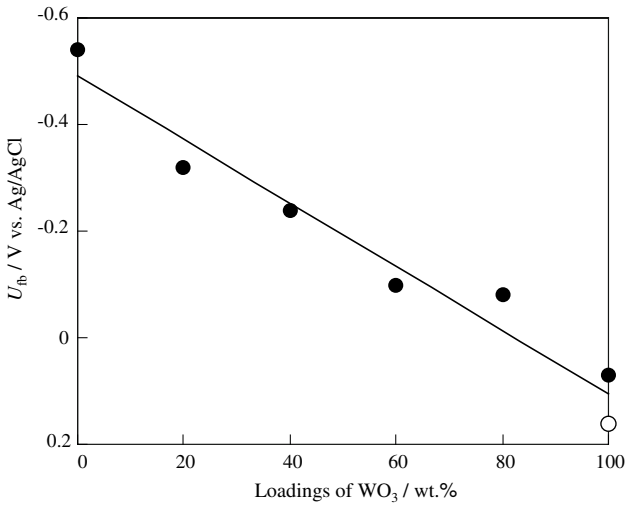

Fig. 9 Dependence of the flat band potentials as a function of loadings of WO_3 on TiO_2. White circle shows the flatband potential of a-WO_3. The pH of an aqueous solution was adjusted at 2.1

towards the positive potential from −0.54 V to +0.07 V as an increase of loadings of WO_3 as shown in Fig. 9.

As shown in Fig. 10, it was observed that the photocurrent efficiency for the film electrodes is not influenced by the pH of aqueous solutions.

The bandgap energy of TiO_2 was determined to be E_g = 3.40 eV by threshold against energy ($h\nu$) as shown in

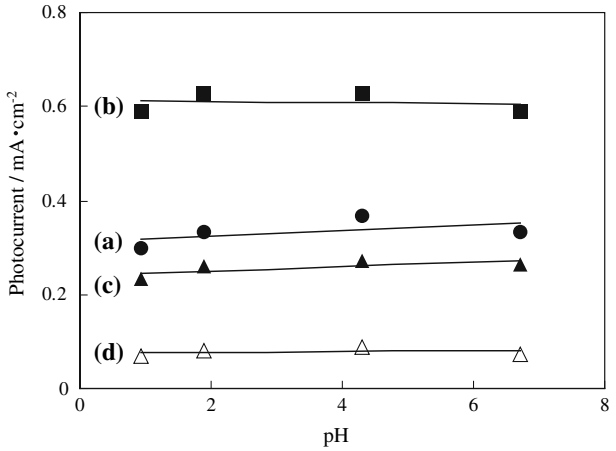

Fig. 10 Dependence of the pH of aqueous solutions on the saturated photocurrent density for TiO_2 (**a**), 40-WO_3/TiO_2 (**b**), c-WO_3 (**c**) and a-WO_3 (**d**)

Fig. 11 [I]. Likewise, the band gaps of 40-WO_3/TiO_2, a-WO_3 and c-WO_3 were estimated to be E_g = 3.35 eV for 40-WO_3/TiO_2, E_g = 3.35 eV for a-WO_3 and E_g = 2.75 eV for c-WO_3, respectively (cf. Fig. 11 [II]) [20]. It is reported that amorphous WO_3 shows larger band-gap energy (3.35 eV) than polycrystalline WO_3 (2.5–2.8 eV) as shown in the reference [13]. The similar phenomena can be also observed in the case of amorphous silicon (1.8 eV) compared with polycrystalline silicon (1.1 eV) [22]. It can be assumed that band-gap widening may be possibly explained by structural fluctuation of amorphous WO_3 or Si. On the other hand, amorphous-like WO_3 can be observed on hybrid WO_3/TiO_2 in the low loadings of WO_3, which cause the band-gap widening of WO_3. Thus, the band-gap widening of amorphous-like WO_3 may be possibly explained by (i) structural fluctuation or (ii) high dispersibility of WO_3 particles on TiO_2 surface.

Taking the results of flatband potentials and band gaps into consideration, the energy band structure for an amorphous-like WO_3 coupled with TiO_2 (a-WO_3/TiO_2) is proposed in Fig. 12. As a whole, the photo-induced holes and electrons on the films participate in the oxidation and the reduction of substrates, respectively. In our system, the electrons go through outer electric circuit towards counter electrode under potential bias, probably causing the reduction of oxygen. The photo-induced electrons and holes effectively transfer to the conduction band of WO_3, and to the valence band of TiO_2, respectively, by accumulating electrons and holes in two different semiconductor mixture layers. In general, the formate anion ($HCOO^-$) can be oxidized by a hole to form HCOO·, followed by automatic oxidation to CO_2, H^+ and e^- from the simple occurrence of the photocurrent doubling [10]. So that, it can be supposed that one photon gives the photoreaction of HCOOH → $CO_2 + 2H^+ + 2e^-$. It can be assumed that photoirradiation of

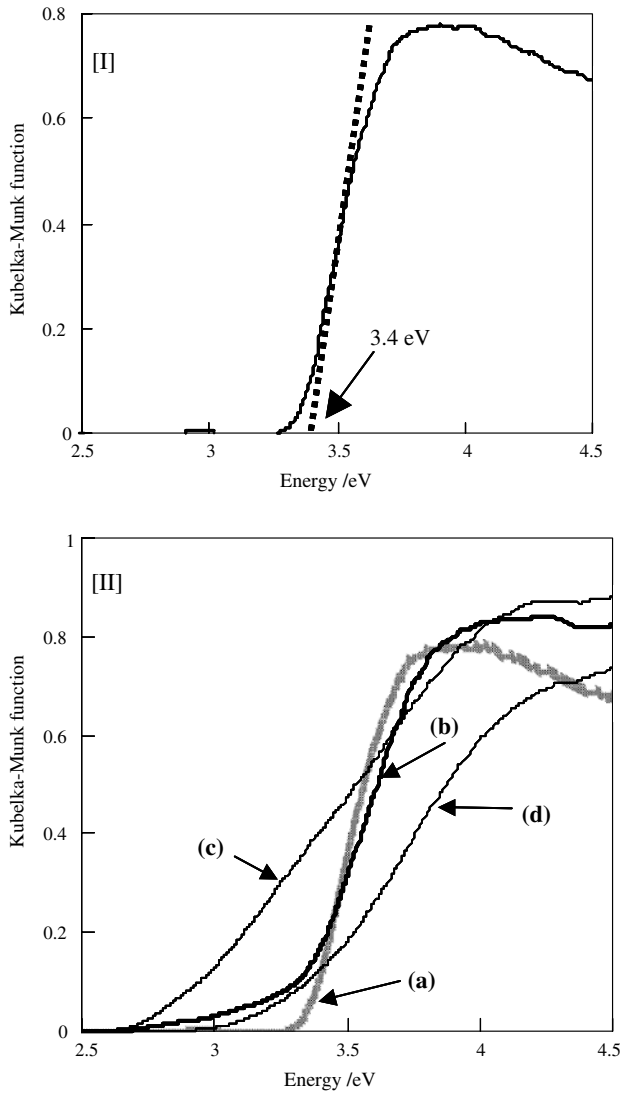

Fig. 11 An estimation of the bandgap of TiO_2 [I], and absorption spectra of TiO_2 (**a**), 40-WO_3/TiO_2 (**b**), c-WO_3 (**c**) and a-WO_3 (**d**) [II]

a-WO_3/TiO_2 gives more effective charge separation ($h^+ \cdots e^-$) than a polycrystalline WO_3 coupled with TiO_2 (c-WO_3/TiO_2), since the potential of valence band of a-WO_3 is more anodic than that of c-WO_3.

4 Conclusions

A hybrid WO_3/TiO_2 film electrode was shown to perform more effective electrochemically assisted photocatalysis (photocurrent efficiency) than either TiO_2 or WO_3 by themselves due to the effective charge separation. In particular, the hybrid WO_3/TiO_2 film having an amorphous-like WO_3 can play an important role in more effective charge separation than the film having a polycrystalline WO_3.

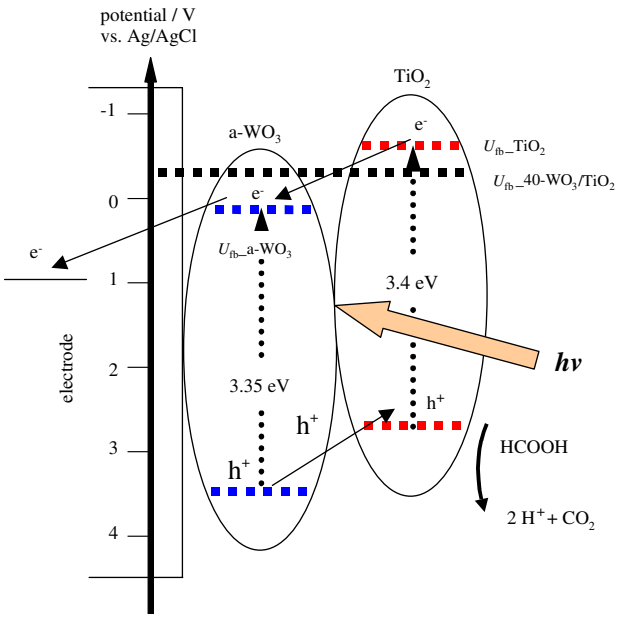

Fig. 12 Schematic energy diagram for the photo-induced charge transfer on the a-WO_3/TiO_2 film electrode. The pH of an aqueous solution was adjusted at 2.1

Acknowledgements We thank Prof. Masakazu Anpo in Osaka Prefecture University for his useful discussion. The research described herein was partially supported by the Yazaki Memorial Foundation for Science & Technology and we would like to express our thanks for their kind assistance.

References

1. Fujishima A, Honda K (1972) Nature 238:37–38
2. Anpo M, Dohshi S, Kitano M, Hu Y (2006) Chem Ind 108: 595–622
3. Hashimoto K, Irie H, Fujishima A (2005) Jpn J Appl Phys 44:8269–8285
4. Zhao J, Chen C, Ma W (2005) Top Catal 35:269–278
5. Yamashita H, Takeuchi M, Anpo M (2004) Encyclopedia Nanosci Nanotechnol 10:639–654
6. Li W, Shah I, (2004) Encyclopedia Nanosci Nanotechnol 9: 669–695
7. Kamat PV (1993) Chem Rev 93:267–300
8. Wang R, Hashimoto K, Fujishima A, Chikuni M, Kojima E, Kitamura A, Shimohigoshi M, Watanabe T (1997) Nature 388:431–432
9. Santato C, Odziemkowski M, Ulmann M, Augustynski J (2001) J Am Chem Soc 123:10639–10649
10. Santato C, Ulmann M, Augustynski J (2001) J Phys Chem B 105:936–940
11. Nagasu M, Koshida N (1990) Appl Phys Lett 57:1324–1325
12. Kikuchi E, Iida K, Fujishima A (1993) J Electroanal Chem 351:105–114
13. Shiyanovskaya I, Hepel M (1999) J Electrochem Soc 146: 243–249
14. Bedja I, Hotchandani S, Kamat PV (1993) J Phys Chem 97(42):11064–11070
15. He T, Ma Y, Cao Y, Hu X, Liu H, Zhang G, Yang W, Yao J (2002) J Phys Chem B 196:12670–12676
16. Ngaotrakanwiwat P, Tatsuma T, Saitoh S, Ohko Y, Fujishima A (2003) Phys Chem Chem Phys 5:3234–3237

17. Tatsuma T, Saitoh S, Ohko Y, Fujishima A (2001) Chem Mater 13:2838–2842
18. Hauch A, Georg A, Krašovec UO, Orel B (2002) J Electrochem Soc 149:A1208–A1211
19. Higashimoto S, Kitahata N, Mori K, Azuma M (2005) Catal Lett 101:49–51
20. Higashimoto S, Makoto MS, Azuma M (2006) Thin Solid Films 503:201–206
21. Gavrilyuk AI, Prokhvatilov VG, Chudnovskiĭ A (1982) Sov Phys Solid State 24:558–563
22. Lim DG, Kim HW, Lee SE, Yi J (1998) European Commission, 2nd World Conference on Photovoltaic Solar Energy Conversion, Vol. I, pp 890–893